MIT Joint Program on the Science and Policy of Global Change

GLOBAL

SCIENCE   POLICY

CHANGE

M I T

Estimated PDFs of Climate System Properties Including Natural and Anthropogenic Forcings

Chris E. Forest, Peter H. Stone and Andrei P. Sokolov

Report No. 126
September 2005

The MIT Joint Program on the Science and Policy of Global Change is an organization for research, independent policy analysis, and public education in global environmental change. It seeks to provide leadership in understanding scientific, economic, and ecological aspects of this difficult issue, and combining them into policy assessments that serve the needs of ongoing national and international discussions. To this end, the Program brings together an interdisciplinary group from two established research centers at MIT: the Center for Global Change Science (CGCS) and the Center for Energy and Environmental Policy Research (CEEPR). These two centers bridge many key areas of the needed intellectual work, and additional essential areas are covered by other MIT departments, by collaboration with the Ecosystems Center of the Marine Biology Laboratory (MBL) at Woods Hole, and by short- and long-term visitors to the Program. The Program involves sponsorship and active participation by industry, government, and non-profit organizations.

To inform processes of policy development and implementation, climate change research needs to focus on improving the prediction of those variables that are most relevant to economic, social, and environmental effects. In turn, the greenhouse gas and atmospheric aerosol assumptions underlying climate analysis need to be related to the economic, technological, and political forces that drive emissions, and to the results of international agreements and mitigation. Further, assessments of possible societal and ecosystem impacts, and analysis of mitigation strategies, need to be based on realistic evaluation of the uncertainties of climate science.

This report is one of a series intended to communicate research results and improve public understanding of climate issues, thereby contributing to informed debate about the climate issue, the uncertainties, and the economic and social implications of policy alternatives. Titles in the Report Series to date are listed on the inside back cover.

Henry D. Jacoby and Ronald G. Prinn,
Program Co-Directors

For more information, please contact the Joint Program Office

Postal Address: Joint Program on the Science and Policy of Global Change
77 Massachusetts Avenue
MIT E40-428
Cambridge MA 02139-4307 (USA)

Location: One Amherst Street, Cambridge
Building E40, Room 428
Massachusetts Institute of Technology

Access: Phone: (617) 253-7492
Fax: (617) 253-9845
E-mail: globalchange@mit.edu
Web site: http://MIT.EDU/globalchange/

♻ *Printed on recycled paper*

Estimated PDFs of Climate System Properties Including Natural and Anthropogenic Forcings

Chris E. Forest, Peter H. Stone and Andrei P. Sokolov

Abstract

We present revised probability density functions (PDF) for climate system properties (climate sensitivity, rate of deep-ocean heat uptake, and the net aerosol forcing strength) that include the effect on 20th century temperature changes of natural as well as anthropogenic forcings. The additional natural forcings, primarily the cooling by volcanic eruptions, affect the PDF by requiring a higher climate sensitivity and a lower rate of deep-ocean heat uptake to reproduce the observed temperature changes. The estimated 90% range of climate sensitivity is 2.4 to 9.2 K. The net aerosol forcing strength for the 1980s decade shifted towards positive values to compensate for the now included volcanic forcing with 90% bounds of –0.7 to –0.16 W/m². The rate of deep-ocean heat uptake is also reduced with the effective diffusivity, Kv, ranging from 0.25 to 7.3 cm²/s. This upper bound implies that many coupled atmosphere-ocean GCMs mix heat into the deep ocean (below the mixed layer) too efficiently.

Contents

1   Introduction

Forest *et al.* (2002) presented an estimate of the joint probability density function (pdf) for uncertain climate system properties. Other groups (Andronova & Schlesinger, 2001; Gregory *et al.*, 2002; Knutti *et al.*, 2003) have estimated similar pdfs although each uses different methods and data. However all are based on estimating the degree to which a climate model can reproduce the historical climate record. Parameters within each model are perturbed to alter the response to climate forcings and a statistical comparison is used to reject combinations of model parameters.

We use an optimal fingerprint detection technique for comparing model and observational data. This technique consists of running a climate model under a set of prescribed forcings and using climate change detection diagnostics to determine whether the simulated climate change is observed in the climate record and is distinguishable from unforced variability of the climate system (see Mitchell *et al.* (2001) or International *ad hoc* Detection and Attribution Group (2005) and references therein). As is well known, it is not possible to estimate the true climate system variability on longer time scales from observations and therefore, climate models are run with fixed boundary conditions for thousands of years to obtain an estimate of the climate variability.

Forest *et al.* (2000, 2001, 2002) developed a method using the MIT 2D model to analyze uncertainty in climate sensitivity (S), the rate of heat uptake by the deep ocean (K_v), and the net aerosol forcing (F_{aer}). These factors ($\theta = S, K_v, F_{aer}$) were jointly constrained by using three different diagnostics to estimate the probability of rejection for combinations of model parameters that lead to simulations of the 20th century which are inconsistent with the observed records of climate change. The individual probability density functions (pdfs) can be combined to provide stronger constraints for the uncertain properties via an application of Bayes' Theorem. A 2D model is required because 3D models are computationally too inefficient.

Our former analysis only took into account anthropogenic forcings by greenhouse gases, stratospheric ozone, and aerosols. We now also take into account the change in radiative forcing by solar irradiance fluctuations, by stratospheric aerosols due to volcanic eruptions, and by land-use and land-cover vegetation changes. The major uncertain forcing is that due to sulfate aerosols, so in our earlier study, the sulfate aerosol pattern had a specified dependence on latitude and surface type, but the amplitude was taken to be one of the uncertain parameters to be constrained. There are additional uncertainties associated with the new forcings that we now include, but they are generally believed to be smaller than the uncertainties associated with sulfate aerosols (Hansen *et al.*, 2002). Thus, in our new analysis, we retain the amplitude of the sulfate aerosol forcing as the only uncertain

parameter describing the forcing. However, we do include in this paper some tests of whether our new results are sensitive to uncertainties in the new forcings.

2 Methodology

To quantify uncertainty in climate model properties, the basic method (Forest *et al.*, 2001, 2002) can be summarized as consisting of two parts: simulations of the 20th century climate record and the comparison of the simulations with observations using optimal fingerprint diagnostics. First, we require a large sample of simulated records of climate change in which climate parameters have been systematically varied. This requires a computationally efficient model with variable parameters as provided by the MIT 2D statistical-dynamical climate model (Sokolov & Stone, 1998). A brief description of the MIT 2D climate model and its recent modifications are given in supplemental material. Second, we employ a method of comparing model data to observations that appropriately filters "noise" from the pattern of climate change. The variant of optimal fingerprinting proposed by Allen & Tett (1999) provides this tool and yields detection diagnostics that are objective estimates of model-data goodness-of-fit. These goodness of fit statistics are then used to estimate the likely value of uncertain parameters (via a likelihood function, $L(\theta)$) for multiple diagnostics of climate change. Individual $L(\theta)$ are then combined to estimate the posterior distribution, $p(\theta|\Delta T_i, C_N)$, where ΔT_i represent the three temperature change patterns and C_N is the noise covariance matrix required to estimate the goodness-of-fit statistics.

In this work, the noise covariance matrix has been estimated from multiple control runs of AOGCMs. (The noise estimate for deep ocean heat uptake also includes analysis error estimates from Levitus *et al.* (2000).) The matrix represents the natural variability in any predicted pattern which is determined by the variability in the corresponding pattern amplitude in successive segments of "pseudo-observations" extracted from the control run for the climate model. The variability of the MIT 2D climate model is somewhat lower than that of AOGCMs (Sokolov & Stone, 1998), but the model does exhibit changes in variability which are dependent on S and K_v and are similar to results from Wigley & Raper (1990).

2.1 Experimental Design

The description of the climate model experiments, the ensemble design, and the algorithm for estimating the joint PDFs are provided in full in Forest *et al.* (2001, 2002). The major change in the new experiments is the inclusion of three additional 20th century forcings during the period 1860-1995. The set of forcings is now: greenhouse gas concentrations,

sulfate aerosol loadings, tropospheric and stratospheric ozone concentrations, land-use vegetation changes (Ramankutty & Foley, 1999), solar irradiance changes (Lean, 2000), and stratospheric aerosols from volcanic eruptions (Sato *et al.*, 1993). We refer to these forcings as GSOLSV with the first three, GSO, being those used in Forest *et al.* (2002). (Details on all forcings are in the supplement.)

Additionally, we elected to run each perturbation of the 4 member ensemble starting with different initial conditions in 1860 rather than perturbing the climate system in 1940 as done previously. This provides data for each ensemble member for the entire simulation as we will be using surface temperatures beginning in 1906. The initial conditions for each ensemble member were taken every ten years from an equilibrium control simulation. This results in 4x136 = 544 simulation years for each choice of model parameters.

3   Results

In the simulated climate change, the additional forcings have two major effects that can be illustrated by examining the simulated response to the GSOLSV and GSO forcings and comparing with the observed records, directly (Fig. 1). For the "best fit" parameters in each case, the new results require higher S and slightly weaker F_{aer}. This shift in the "best fit" parameters results in appropriate shifts in the distributions and are summarized as follows. The inclusion of the volcanic aerosol forcing provides a net surface cooling during the latter 20th century (Fig. 1). This requires changes in uncertain model parameters to remain consistent with the historical climate record (Figs. 2 and 3) which can be achieved by reducing K_v or F_{aer}, increasing S, or combinations of all three. The median net aerosol forcing is partially reduced from -0.6 to -0.4 W/m^2 but there is little change in the width of the distribution with the 5-95%-ile range being 0.6 W/m^2. The reduction in the median is partially because the net aerosol forcing no longer includes the volcanic term. However, the net aerosol forcing remains a cooling effect. The medians for S, K_v, and F_{aer} are 3.1 K, 1.4 cm^2/s, and -0.35 W/m^2, respectively, for the distributions using an expert prior on S as used in Forest *et al.* (2002).

The new distributions are compared with that of Forest *et al.* (2002) in Fig. 2 and two key comparisons are made. In one, we compare the distributions with identical treatments of the climate change diagnostics by keeping the number of retained EOFs (κ) in the decomposition of $C_N^{-1}(\kappa)$ fixed. Thus, for the surface temperature diagnostic, we use $\kappa_{sfc} = 14$ in both the GSO and GSOLSV pdfs and the marginal posterior distributions for S, F_{aer}, and K_v are altered. In the second comparison, we allow κ_{sfc} to vary. In Forest *et al.* (2002) for the surface data, we found that we could reject $\kappa_{sfc} > 14$ based on the Allen & Tett (1999) criterion. With the additional forcings, we are no longer able to reject

the higher EOFs and find that the distributions are insensitive for $15 < \kappa_{sfc} < 19$. In a separate work on Bayesian selection criteria, Curry *et al.* (2005) using our data find that a break occurs at $\kappa_{sfc} = 16$ and thus we select this as an appropriate cutoff. This inclusion of higher order EOFs is equivalent to stating that smaller spatial and temporal scale patterns (in five decadal means and four equal-area zonal averages) found in the GSOLSV response are significant, unlike the GSO case. This also implies that the observations show this behavior. As a final issue, this shift from $\kappa_{sfc} = 14$ to 15 further limits the higher K_v values. We note that the range of effective ocean diffusivities for the existing AOGCMs is 4-25 cm^2/s (Sokolov *et al.*, 2003) and these values appear to be highly unlikely according to our new results. (We note that a more recent analysis of the deep ocean temperatures (Levitus *et al.*, 2005) has a 20% weaker trend during the period used in our analysis. This would require even lower acceptable K_v values.)

Several sensitivity tests were performed to assess the robustness of the estimated distributions. Specifics are found in the supplemental information but we briefly discuss two here. A first test was designed to determine whether the location of the deep-ocean heat uptake influenced the spatio-temporal patterns of temperature change. The latitude dependence of K_v, which was based on observations of Tritium mixing (Sokolov & Stone, 1998), was changed to reflect the pattern identified in the ocean data (Levitus *et al.*, 2000). Although local surface temperatures were changed, the large-scale averages (four equal-area zonal bands) as used in our diagnostics were not affected. A second test explored the sensitivity of the results to reducing the strength of the volcanic forcing by 25%. This requires slightly higher F_{aer} and lower S values to bring the temperature response down to match the observations but the changes are relatively small. These results suggest that the PDFs are robust to such changes.

As discussed earlier, the estimated distributions depend on the choice of the truncation for the eigen-decomposition of C_N for the surface temperature diagnostic. We also tested the choice of AOGCM for estimating C_N. In Forest *et al.* (2002), we used the natural variability as estimated from the HadCM2 and GFDL_R30 AOGCMs. In our new results, we have used diagnostics based on the natural variability from control runs by the HadCM2, HadCM3, GFDL_R30, and PCM models. The resulting pdfs have not differed qualitatively (shown in supplemental material). Although the results are not sensitive to the choice of AOGCM, observations do not exist to test the quality of such estimates.

4   Discussion and Conclusions

We present a revised estimate of the pdfs for climate system properties that now includes the response to both natural and anthropogenic forcings. With additional new forcings, a

larger climate sensitivity and a reduced rate of ocean heat uptake below the mixed layer are required to match the observed climate record in the 20th century. The primary factor leading to this change is the strong cooling forcing by volcanic eruptions through the stratospheric aerosols. Similarly, there is a small change in the aerosol forcing which tends to offset the volcanic cooling. When using uniform priors on all parameters, these new results are summarized by the 90% confidence bounds of 2.4 to 9.2 K for climate sensitivity, 0.25 to 7.3 cm^2/s for K_v, and -0.7 to -0.16 W/m^2 for the net aerosol forcing strength. When an expert prior for S is used, the 90% confidence intervals are 2.2 to 5.2 K, 0.1 to 5.5 cm^2/s, and -0.62 to -0.05 W/m^2 for S, K_v, and F_{aer}, respectively. Our new results for K_v imply that most AOGCMs are mixing heat into the deep ocean too efficiently, as shown in Fig. 3.

From the two sensitivity tests regarding the strength of the volcanic forcing and the location of the ocean heat uptake, we find that our results appear robust. We also explored the sensitivity to the estimated $C_N^{-1}(\kappa)$ and find that although the specific AOGCM is not very important, the method for truncating the number of retained eigenvectors (i.e., patterns of unforced variability) is critical. For the surface temperature diagnostic, critical changes in the joint PDF occur when κ_{sfc} changes from 14 to 15 and from 19 to 20 and based on Allen & Tett (1999), we cannot reject these higher modes of variability. Marginal likelihood results are promising (Curry *et al.*, 2005, from) yet do not appear to be definitive. Based on κ_{sfc} = 14, 15, or 20, the robust result is that the lower bound on S is higher and failure to reject $S > 5$ K remains. Additionally, for all three choices, high K_v values are rejected as producing too much ocean heat uptake and the net aerosol forcing uncertainty remains stable. Given these considerations, the best choice appears to be κ_{sfc}=15.

Finally, the use of the expert prior on S remains a key factor in limiting the possibility of high values of S. Despite their uncertainties, the paleoclimate results provide data not directly included in the present framework and this supports using a prior influenced by such results. The implications of these results are that the climate system response will be stronger (specifically, a higher lower bound) for a given forcing scenario than previously estimated via the uncertainty propagation techniques in Webster *et al.* (2003).

References

Allen, M. R., & Tett, S. F. B. 1999. Checking for model consistency in optimal fingerprinting. *Clim. Dyn.*, **15**, 419–434.

Andronova, N. G., & Schlesinger, M. E. 2001. Objective Estimation of the Probability Density Function for Climate Sensitivity. *J. Geophys. Res.*, **106**(D19), 22,605–22,612.

Curry, C. T., Sanso, B., & Forest, C. E. 2005. Inference for Climate System Properties. in prep.

Forest, C. E., Allen, M. R., Stone, P. H., & Sokolov, A. P. 2000. Constraining uncertainties in climate models using climate change detection methods. *Geophys. Res. Let.*, **27**(4), 569–572.

Forest, C. E., Allen, M. R., Sokolov, A. P., & Stone, P. H. 2001. Constraining Climate Model Properties Using Optimal Fingerprint Detection Methods. *Clim. Dynamics*, **18**, 277–295.

Forest, C. E., Stone, P. H., Sokolov, A. P., Allen, M. R., & Webster, M. D. 2002. Quantifying uncertainties in climate system properties with the use of recent climate observations. *Science*, **295**, 113–117.

Gregory, J.M., Stouffer, R.J., Raper, S.C.B., Stott, P.A., & Rayner, N.A. 2002. An Observationally Based Estimate of the Climate Sensitivity. *J. Climate*, **15**(22), 3117–3121.

Hansen, J., Sato, M., Nazarenko, L., Ruedy, R., Lacis, A., Koch, D., Tegen, I., Hall, T., Shindell, D., Santer, B., Stone, P., Novakov, T., Thomason, L., Wang, R., Wang, Y., Jacob, D., Hollandsworth, S., Bishop, L., Logan, J., Thompson, A., Stolarski, R., Lean, J., Willson, R., Levitus, S., Antonov, J., Rayner, N., Parker, D., & Christy, J. 2002. Climate Forcings in GISS SI2000 Simulations. *J. Geophys. Res.*, **107**, DOI 10.1029/2001JD001143.

International *ad hoc* Detection and Attribution Group, [Contributing members: T. Barnett, F. Zwiers, G. Hegerl, M. Allen, T. Crowley (coordinator), N. Gillett, K. Hasselmann, P. Jones, B. Santer, R. Schnur, P. Stott, K. Taylor, S. Tett]. 2005. Detecting and Attributing External Influences on the Climate System: A Review of Recent Advances. *J. Climate*, **18**(9), 1291–1314.

Jones, P. D. 2000. *http://www.cru.uea.ac.uk/cru/data/temperat.htm*. University of East Anglia, Climate Research Unit.

Knutti, R., Stocker, T. F., Joos, F., & Plattner, G.-K. 2003. Probabilistic climate change projections using neural networks. *Clim. Dyn.*, **21**, 257–272.

Lean, J. 2000. Evolution of the Sun's Spectral Irradiance Since the Maunder Minimum. *Geophys. Res. Lett.*, **27**, 2421–2424.

Levitus, S., Antonov, J., Boyer, T. P., & Stephens, C. 2000. Warming of the World Ocean. *Science*, **287**, 2225–2229.

Levitus, S., Antonov, J., & Boyer, T. P. 2005. Warming of the World Ocean, 1955–2003. *Geophys. Res. Let.*, **32**(L02604), doi:10.1029/2004GL021592.

Mitchell, J. F. B., Karoly, D. J., Hegerl, G. C., Zwiers, F. W., Allen, M. R., & Marengo, J. 2001. Detection of Climate Change and Attribution of Causes. *Pages 695–738 of:* Houghton, J. T., Ding, Y., Griggs, D. J., Noguer, M., van der Linden, P. J., Dai, X., Maskell, K., & Johnson, C. A. (eds), *Climate Change 2001: The Scientific Basis*. Cambridge University Press, Cambridge, UK and New York, NY, USA.

Ramankutty, N., & Foley, J. A. 1999. Estimating historical changes in global land cover: croplands from 1700 to 1992. *Global Biogeochemical Cycles*, **13**(4), 997–1027.

Sato, M., Hansen, J. E., McCormick, M. P., & Pollack, J. B. 1993. Stratospheric aerosol optical depths. *J. Geophys. Res.*, **98**, 22987–22994.

Sokolov, A. P., & Stone, P. H. 1998. A flexible climate model for use in integrated assessments. *Clim. Dyn.*, **14**, 291–303.

Sokolov, A. P., Forest, C. E., & Stone, P. H. 2003. Comparing Oceanic Heat Uptake in AOGCM Transient Climate Change Experiments. *J. Climate*, **16**, 1573–1582.

Webster, M., Forest, C., Reilly, J., Babiker, M., Mayer, M., Prinn, R., Sarofim, M., Sokolov, A., Stone, P., & Wang, C. 2003. Uncertainty Analysis of Climate Change and Policy Response. *Climatic Change*, 295–320.

Wigley, T. M. L., & Raper, S. C. B. 1990. Natural variability of the climate system and detection of the greenhouse effect. *Nature*, **344**, 324–327.
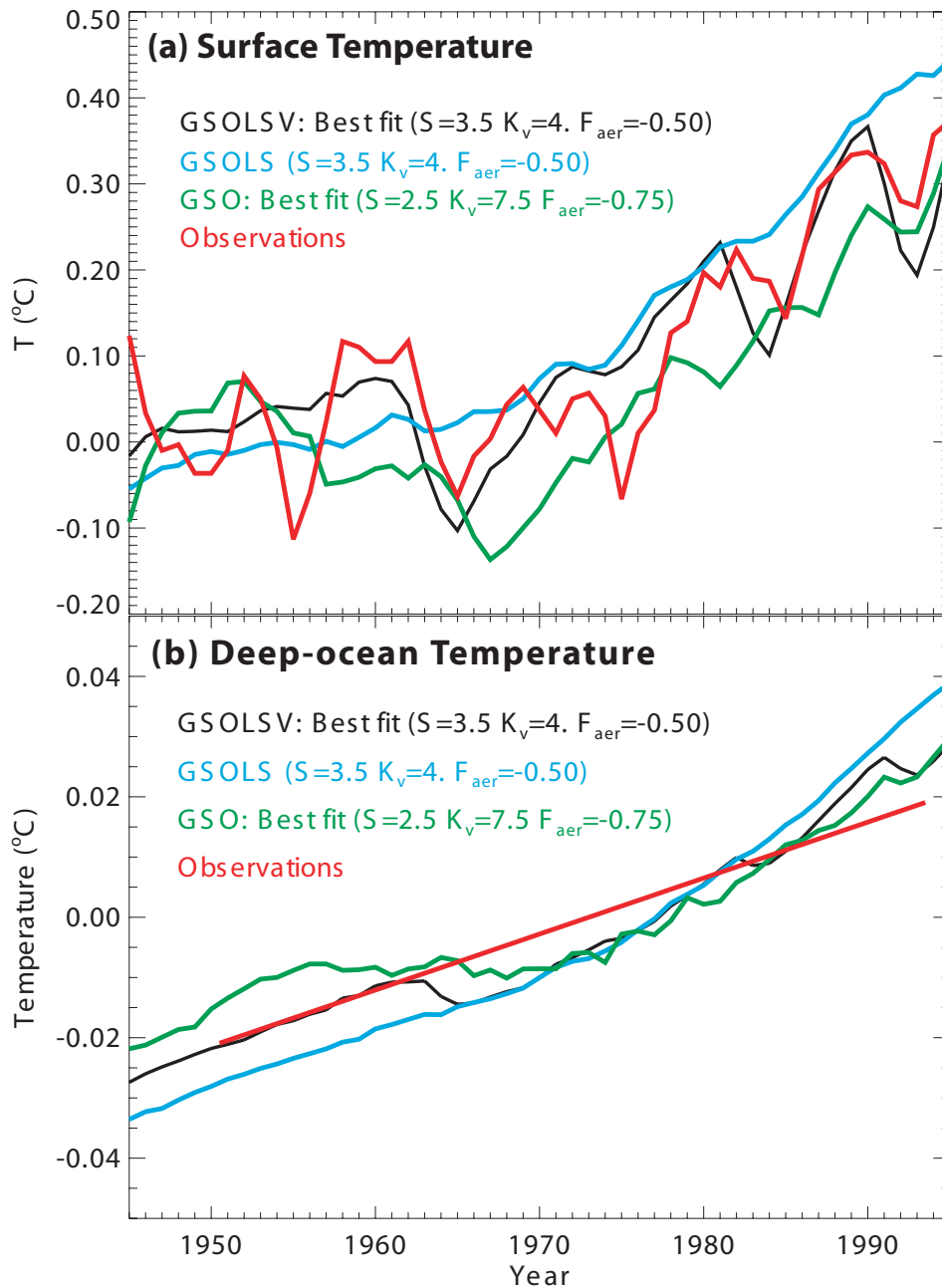
Figure 1: Representative MIT 2D model simulations with the GSOLSV, GSOLS, and GSO forcings for **(a)** global-mean annual-mean surface temperature change, and **(b)** 0 to 3 km global mean annual-mean ocean temperature change. We show cases near the distributions' modes for GSOLSV (black) and GSOLS (blue) with $S = 3.5$ K, $K_v = 4$ cm^2/s, and $F_{aer} = -0.5$ W/m^2 and for GSO (green) with $S = 2.5$ K, $K_v = 7.5$ cm^2/s, and $F_{aer} = -0.75$ W/m^2. Observations (red) from Jones (2000) (surface) and Levitus *et al.* (2000) (deep-ocean). Surface temperatures have been smoothed with a three-point moving average.
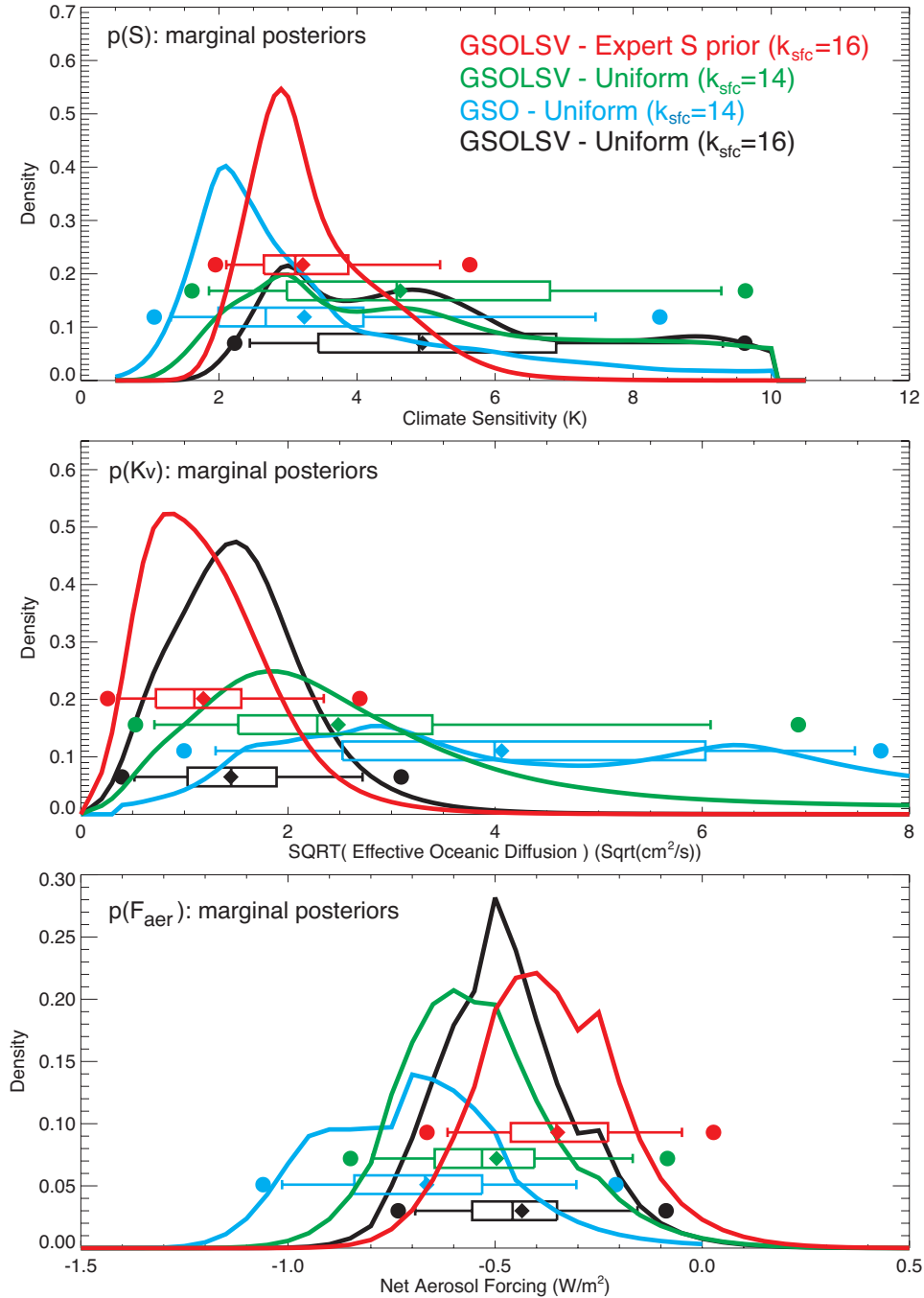
Figure 2: The marginal *posterior* probability density function for the three climate system properties for four cases. In each panel, the marginal pdfs are shown for the GSOLSV forcings with $\kappa_{sfc} = 16$ (black) and 14 (green) and for GSO case (blue) with $\kappa_{sfc} = 14$ from Forest *et al.* (2002). A fourth case (red) includes an expert prior on *S* and uniform priors elsewhere with $\kappa_{sfc} = 16$. Marginal distributions are estimated by integrating the density function over the remaining two parameters and renormalizing. The whisker plots indicate boundaries for the percentiles 2.5 to 97.5 (dots), 5 to 95 (vertical bar at ends), 25 to 75 (box ends), and 50 (vertical bar in box). The mean is indicated with the diamond and the mode is the peak in the distribution.
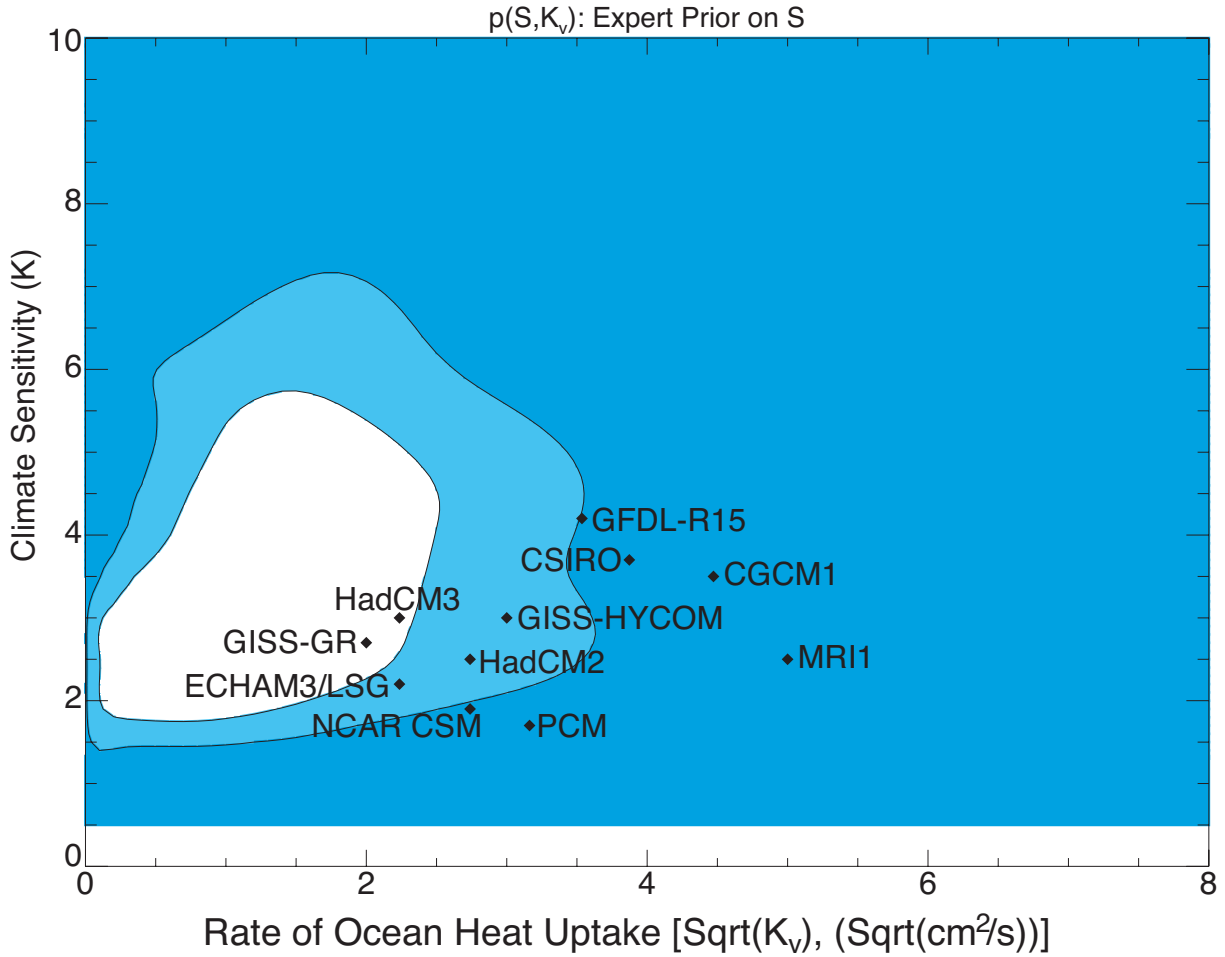
Figure 3: The marginal *posterior* probability density function for GSOLSV results with expert prior on *S* for the *S-K_v* parameter space. The blue shading denotes rejection regions for a given significance level: 10% (light) and 1% (dark). The positions of AOGCMs (from Sokolov *et al.*, 2003) represent the parameters in the MIT 2D model that match the transient response in surface temperature and thermal expansion component of sea-level rise under a common forcing scenario. Lower *K_v* values imply less deep-ocean heat uptake and hence, a smaller effective heat capacity of the ocean.

Supplement to: Estimated PDFs of climate system properties including natural and anthropogenic forcings

Chris E. Forest and Peter H. Stone and Andrei P. Sokolov

This supplement provides additional information for Forest *et al.* (2005). It presents details on the methods used (Sect. 1) and a set of sensitivity tests for the estimated PDFs (Sect. 2). Three tests provide details on sensitivies to the noise model truncation, to the latitude dependence of the deep-ocean heat uptake, and to uncertainty in the volcanic forcing. There is also a section on the ability of the 2D climate model to reproduce the ocean heat uptake in response to the 20th century forcings.

1 Methods

1.1 Summary of PDF Estimation Algorithm

The following steps provide further details of the method for estimating the probability density functions (PDFs):

1. Simulate 20th century climate using anthropogenic and natural forcings while systematically varying the choices of climate system properties, $\theta = \{S, K_v, F_{aer}\}$, as set in the MIT 2D climate model, where S is the climate sensitivity (defined as the equilibrium change in surface air temperature when the CO_2 concentration doubles), K_v is an effective vertical diffusivity controlling the rate at which heat anomalies penetrate into the deep ocean (below the mixed layer), and F_{aer} is the net aerosol forcing and represents the uncertainty in the net historical forcing.

2. Compare the spatio-temporal patterns of climate change in each model temperature response, $T(\theta)$, against observed patterns, T_{obs}, as in an optimal fingerprint detection algorithm using unforced variability estimated from AOGCMs to obtain an estimate, $C_N(\kappa)$, of the covariance matrix and only the first κ modes of variability are retained from the eigenvalue decomposition. The best choice of κ is discussed later. The observed temperature change diagnostics that we use are described in Appendix A2.

3. Use the goodness-of-fit statistics, $r^2(\theta, T_{obs}) = (T(\theta) - T_{obs})^T C_N^{-1}(\kappa)(T(\theta) - T_{obs})$, to obtain the likelihood function, $L(\theta) = p(T_{obs}|\theta, C_N)$ for each $T(\theta)$ diagnostics. This likelihood is based on the result that r^2 must differ by $mF_{m,\nu}$, for a given significance level, to be considered different from the minimum r^2 value (Forest *et al.*, 2001). The minimum r^2 is estimated as where the model obtains its best-fit with observations for each diagnostic and also has uncertainties.

4. Use Bayes theorem to estimate the joint distribution $p(\theta|T_{obs}, C_N)$ that results from combining the likelihood functions for each diagnostic.

We note that this algorithm has similar features to those of both Andronova & Schlesinger (2001) and Gregory *et al.* (2002) with differences arising in different choices of climate models and observational data. Only the Forest *et al.* (2002) approach uses spatio-temporal patterns of climate change that are integral to the optimal fingerprint detection algorithm (e.g., Allen & Tett, 1999). The resulting posterior pdf then determines the regions of the parameter space, θ, that can be rejected as being inconsistent with the multiple observational data sets.

1.2   Description of MIT 2D Climate Model

The MIT 2D climate model consists of a zonally averaged atmospheric model coupled to a mixed-layer Q-flux ocean model, with heat anomalies diffused below the mixed-layer. The model details can be found in Sokolov & Stone (1998). The atmospheric model is a zonally averaged version of the Goddard Institute for Space Studies (GISS) Model II general circulation model (Hansen *et al.*, 1983) with parameterizations of the eddy transports of momentum, heat, and moisture by baroclinic eddies (Stone & Yao, 1987, 1990). The model version we use has 46 latitude bands ($\Delta\phi = 4^o$) and 11 vertical layers with 4 layers above the tropopause. The 8°latitudinal resolution used in our earlier study was improved to 4°mainly to allow for smoother transitions of melting sea-ice in high latitudes.

The model also employs a 2.5D Q-flux ocean mixed layer model with 4°x 5°latitude-longitude grid cells and diffusion of heat anomalies into the deep-ocean below the climatological mixed layer. Allowing for changing sea-ice in multiple grid cells, this provides smoother melt transitions than before. This ocean component model is described by Hansen *et al.* (1983) and only increased computations by a few percent. The model uses the GISS radiative transfer code which contains all radiatively important trace gases as well as aerosols and their effect on radiative transfer. The surface area of each latitude band is divided into a percentage of land, ocean, land-ice, and sea-ice with the surface fluxes computed separately for each surface type. This allows for appropriate treatment of radiative forcings dependent on underlying surface type such as anthropogenic aerosols. The atmospheric component of the model, therefore, provides most important nonlinear interactions between components of the atmospheric system.

The MIT model has two parameters that determine the timescale and magnitude of the decadal to century timescale response to an external forcing. These are the equilibrium climate sensitivity (S) to a doubling of CO_2 concentrations and the global-mean vertical thermal diffusivity (K_v) for the mixing of thermal anomalies into the deep ocean. Sokolov & Stone (1998) have shown that the large-scale response of a given 3D AOGCM can be duplicated by the MIT 2D model with an appropriate choice of these two parameters for any forcing (see supplemental material, section 2.2). Published values of 3D AOGCM model sensitivities range from 2.0°to 5.1°C (Cubasch *et al.*, 2001). Comparisons between time-series of transient climate changes calculated with the MIT model and with 3D AOGCMs show that the GCM's equivalent vertical diffusivities range from 4.0 to 25.0 cm^2/s (see Figure 3 in the main text). The model's flexibility to duplicate AOGCM responses, along with its computational efficiency, provides the tool needed for exploring questions which would be impractical to explore with 3D AOGCMs.

1.3   Temperature Change Diagnostics

We have elected to use the same climate change diagnostics as used in Forest *et al.* (2002). This allows us to isolate the effect of the additional forcings on the posterior distributions. The climate change diagnostics used in Forest *et al.* (2002) were:

- **Surface temperatures:** 4 equal-area latitude averages for each of five decades from 1946–1995 referenced to 1905-1995 climatology. Source: Jones (2000)

- **Deep-ocean temperatures:** trend in global-mean 0–3km deep layer of pentadal av-

Table 1: Comparison of applied forcings for GSO and GSOLSV scenarios.

	GSO (Forest *et al.*, 2001, 2002)	GSOLSV (This study.)
G	Radiative forcing by greenhouse gases prescribed as equivalent CO_2 concentrations	All greenhouse gas concentrations specified explicitly
S	Sulfate aerosol loading scaled by historical sulfur emissions (Hameed & Dignon, 1992)	Updated historical sulfur emissions to Smith *et al.* (2003)
O	Stratospheric and tropospheric ozone concentrations specifed from 1979-1995	Stratospheric and tropospheric ozone specified from 1860-2001 (Hansen *et al.*, 2002)
L	N/A	Land-use and land-cover change (Ramankutty & Foley, 1999)
S	N/A	Solar irradiance change including secular change. (Lean, 2000)
V	N/A	Volcanic forcing specified as stratospheric aerosol optical depth Sato *et al.* (1993) updated to 2001.

erages from 1952–1995. Source: Levitus *et al.* (2000)

- **Upper-air temperatures:** Difference between 1986–1995 and 1961–1980 averages at eight standard pressure levels from 850-50 hPa on 5 degree grid. GSO: Years 1963-4 and 1992 were removed. GSOLSV: all years used. Source: Parker *et al.* (1997)

1.4   Summary of Applied Climate Forcings

The current set of simulations has an updated set of historical climate forcings during the period 1860-1995. The set of forcings is now: greenhouse gas concentrations, sulfate aerosol loadings, tropospheric and stratospheric ozone concentrations, land-use vegetation changes, solar irradiance changes, and stratospheric aerosols from volcanic eruptions. GSOLSV is the shorthand notation for this set of forcings (summarized in Table 1.)

Previously, greenhouse gas concentrations were prescribed as equivalent CO_2 concen-

trations such that the radiative forcing by all gases was converted into a change in the CO_2 concentration alone with all other gases remaining fixed. Now, we specify the concentration of each gas separately. The climate model calculates the historical aerosol forcing prescribed by a change in the surface albedo which depends on the sulfate loadings as a function of latitude. This loading pattern remains fixed but is scaled by the time series of SO_2 emissions to obtain the time varying forcing. In the new simulations, we have updated the SO_2 emissions after 1990 with Smith *et al.* (2003). Previously, the stratospheric and tropospheric ozone concentrations were held constant prior to 1979 and then specified from 1979-1995. Now, we include a historical time series (Hansen *et al.*, 2002) based on GISS estimates of tropospheric ozone in 1890 (Wang & Jacob, 1998). Prior to 1890, the concentrations are held fixed. From 1890 to 1979, a linear interpolation of concentrations were used and after 1979, observed estimates of concentrations were specified. Stratospheric ozone concentrations were held constant prior to 1970, but with a QBO and solar cycle included, and a trend is prescribed for 1970-1979 that is half that in 1979-1996, and observed concentrations from 1979-2001. The stratospheric aerosols from volcanic eruptions are specified as a change in its optical depth for the stratospheric model layers. The solar irradiance changes are from Lean (2000) with the secular trend included. (The ozone, stratospheric aerosol, and solar irradiance forcings are described at http://www.giss.nasa.gov/data/simodel/ and described in Hansen *et al.* (2002).) The land-use vegetation changes (Ramankutty & Foley, 1999) are specifed for 1860-1992 and held fixed after 1992.

2 Sensitivity Tests

2.1 Effects of Noise Model Truncation

The treatment of the noise model is a key element of the detection problem as it represents the noise component in the goodness of fit statistic: $r^2 = \Delta T^T C_N^{-1}(\kappa)\Delta T$ where ΔT is the difference between the model and observed temperature change pattern. $C_N^{-1}(\kappa)$ is the pseudo-inverse (Mardia *et al.*, 1979) in which the eigendecomposition of the noise covariance matrix is used: $C_N = U\Lambda U^T$ with U = matrix of eigenvectors and Λ is the diagonal matrix of eigenvalues, λ_i. This allows us to write: $C_N^{-1}(\kappa) = U^T\Lambda^{-1}U$ where the diagonal elements of Λ^{-1} are $1/\lambda_i$ and the other elements are zero. The truncation must be chosen to retain only the first κ values of Λ^{-1} and thereby eliminating the projection of the temperature change pattern onto those patterns of variability with the smallest variance

in the control run data. Depending on the dimension of the diagnostic, these small λ_i are considered underconstrained and treated as poorly estimated.

We find that the posterior distributions are sensitive to the choice of κ_{sfc} but not for $\kappa_{upper-air}$ and therefore, the selection criteria for κ_{sfc} must be considered. The marginal posteriors (Fig. 1) indicate changes when κ_{sfc} change from 14 to 15 but weak sensitivity to subsequent changes. Based on Allen & Tett (1999), $\kappa_{sfc} = 20$ cannot be rejected, yet a better selection method does not appear available. Using our data, Curry *et al.* (2005) explored an alternative method for choosing κ_{sfc} based on Bayesian methods and find a strong cutoff when κ_{sfc} changes from 18 to 19 and a break in the posteriors when κ_{sfc} changes from 16 to 17. Multiple selection criteria were tested and from the Marginal Likelihood method (Chib & Jeliazhov, 2001), $\kappa_{sfc} = 16$ appears to be an appropriate truncation but both methods give similar results.

We test the sensitivity to the truncation for the surface C_N estimate with $\kappa_{sfc} = 14,15,16$ (Fig. 1a) and $\kappa_{sfc} = 16,18,20$ (Fig. 1b). The PDFs change from 14 to 15, and from 19 to 20, with little change from 15 to 19.

2.2   2D Model Simulation of Ocean Heat Uptake

Sokolov & Stone (1998) compared the performance of the MIT 2D climate model in transient global warming scenarios with the performance of AOGCMs, and showed that the net heat uptake simulated by any given AOGCM could be modeled accuratedly by the 2D model with a choice of S and K_v unique to each AOGCM. In particular, the unique choice worked for different forcing scenarios. However, the scenarios they examined were mostly ones with forcing stronger than that experienced in the 20th century, e.g., CO_2 concentrations increasing 1% per year, or the IPCC IS92a scenario, and none of these included volcanic forcing. Thus, to determine whether the values of S and K_v determined from such scenarios would still simulate accurately the heat uptake by an OGCM in a 20th century scenario, we carried out several simulations in which the 2D ocean model in the MIT 2D model was replaced by a 3D OGCM.

The OGCM used was the MIT OGCM (Marshall *et al.*, 1997) at coarse resolution ($4°$) with conventional subgrid-scale parameterizations. The climate model formed by coupling the standard version of the MIT 2D atmospheric model with this 3D OGCM is documented at "http://web.mit.edu/globalchange/www/MITJPSPGC_Rpt122.pdf". The 2D/3D coupled model was then run in a scenario in which CO_2 increased by 1% per year for 100 years, and the 2D model's S and K_v were picked so that the surface temperature and deep ocean

heat uptake of the 2D model matched the results with the 3D ocean. Then the coupled 2D/3D model and the matching version of the MIT 2D model were both integrated from 1860 to 2100 with identical forcings as further discussed in Sokolov *et al.* (2005). From 1860-1990, all forcings are the same as used in this paper with the net aerosol forcing set to -0.35 W/m^2. From 1991-2100, the model is forced by a reference emission scenario from the MIT EPPA4 emissions model and yields a $\approx$7 W/m^2 net forcing in 2100 with respect to 1990 due to anthropogenic and natural greenhouse gas emissions (for complete details, see Sokolov *et al.*, 2005). The results for the global mean surface temperature and the thermal expansion component of sea-level rise from 1860-2100 are shown in Fig. 2 and indicate that the 2D model closely matches the changes simulated by the coupled 2D/3D model.

2.3   Sensitivity to latitude dependence of ocean heat uptake

In the MIT 2D climate model, heat anomalies in the mixed layer are diffused into the deep-ocean (below the climatological mixed layer) based on a latitude dependent profile, $K_v(\phi)$. We note that this diffusive process represents all mixing processes and not just a diffusion process in the interior deep-ocean. In the original Q-flux model (Hansen *et al.*, 1983), $K_v(\phi)$ was based on observations of tritium mixing into the deep ocean. As presented by Sun & Hansen (2003), the changes in ocean heat content with depth for the 1951-1998 period differ from the mixing implied by the tritium distribution. The ocean heat content changes show stronger heat uptake in the tropical and mid-latitude regions as compared to high latitude regions.

We test whether the deep-ocean heat uptake distribution affects the climate change diagnostics by estimating an empirical latitude dependent profile, $K_v'(\phi)$, to reflect the observed changes in ocean heat content (see Fig. 3). This provides a pattern of deep-ocean heat uptake that mimics the observed pattern (Fig. 4).

The effect of using $K_v'(\phi)$ based on the observed ocean heat content changes results in almost no change in the global mean surface temperatures (differing by at most ± 0.05 K). There are very minor differences in the response and they have very little effect on the large-scale averages that are used in the optimal fingerprint analyses to estimate the PDF of the climate system properties. The conditional probability distribution, $p(\theta|T_{obs}, C_N, F_{aer}$ = -0.5 W/m^2) (Figure 5) is virtually unchanged with the new K_v distribution.

We conclude that the spatial distribution of heat-uptake is not a critical component for estimating the $p(\theta|T_{obs}, C_N)$ for climate system properties. Because large-scale averages are used in the analysis, the small regional differences are not affecting the diagnostics.

The ability for AOGCMs to match the observed behavior on smaller scales remains an open research question.

2.4 Sensitivity to Volcanic Forcing Uncertainty

A key difference between the responses to the GSO and GSOLSV forcing scenarios is the strong decrease in global temperature following the volcanic eruptions. The response to the volcanic aerosol distribution has a significant impact on the temperature time-series for a given choice of θ (main text Fig. 1a). The difference in the 10-year running mean is larger than the observational errors for global mean surface temperature and thus, will lead to a shift in the $p(\theta|T_{obs}, C_N)$ that cannot be attributed to unforced variability alone.

As discussed in the main text, the uncertainty in the climate forcings has been treated by changing the amplitude of the sulfate aerosol forcing and maintaining all other forcings at their specified strengths. Given the impact of the volcanic forcing, we test whether the uncertainty in the volcanic forcing has a significant impact on the resulting pdfs. The forcing uncertainty (2σ) has been subjectively assessed as 30%, 20%, and 15% for the Mt. Agung (1964), El Chichon (1982), and Mt. Pinatubo (1992) eruptions (Hansen *et al.*, 2002). We chose to run a cross-section experiment (S-F_{aer}) with constant $K_v = 4.$ cm^2/s and volcanic forcing reduced by 25% to assess whether the uncertainty would have a significant impact on the estimated pdfs. The posteriors (Fig. 6) for GSOLSV and GSOLSV-75 indicate that slightly stronger F_{aer} and lower S are required to match the observations under reduced volcanic forcing. The changes in these two parameters are, however, relatively small.

References

Allen, M. R., & Tett, S. F. B. 1999. Checking for model consistency in optimal fingerprinting. *Clim. Dyn.*, **15**, 419–434.

Andronova, N. G., & Schlesinger, M. E. 2001. Objective Estimation of the Probability Density Function for Climate Sensitivity. *J. Geophys. Res.*, **106**(D19), 22,605–22,612.

Chib, S., & Jeliazhov, I. 2001. Marginal likelihood from the metropolis-hastings output. *J. Am. Stat. Assoc.*, **96**, 270–281.

Cubasch, U., Meehl, G.A., Boer, G.J., Stouffer, R.J., Dix, M., Noda, A., Senior, C.A., Raper, S., & Yap, K.S. 2001. Projections of Future Climate Change. *Page Chap. 9 of:* Houghton, J.T., & Yihui, D. (eds), *Climate Change 2001: The Scientific Basis*. Cambridge University Press, Cambridge, UK.

Curry, C. T., Sanso, B., & Forest, C. E. 2005. Inference for Climate System Properties. in prep.

Forest, C. E., Allen, M. R., Sokolov, A. P., & Stone, P. H. 2001. Constraining Climate Model Properties Using Optimal Fingerprint Detection Methods. *Clim. Dynamics*, **18**, 277–295.

Forest, C. E., Stone, P. H., Sokolov, A. P., Allen, M. R., & Webster, M. D. 2002. Quantifying uncertainties in climate system properties with the use of recent climate observations. *Science*, **295**, 113–117.

Forest, C. E., Stone, P. H., & Sokolov, A. P. 2005. Estimated PDFs of climate system properties including natural and anthropogenic forcings. *Geophys. Res. Let.*, **submitted**.

Gregory, J.M., Stouffer, R.J., Raper, S.C.B., Stott, P.A., & Rayner, N.A. 2002. An Observationally Based Estimate of the Climate Sensitivity. *J. Climate*, **15**(22), 3117–3121.

Hameed, S., & Dignon, J. 1992. Global emissions of nitrogen and sulfur oxides in fossil fuel combustion, 1970-1986. *J. Air Waste Manage. Assoc.*, **42**, 159–163.

Hansen, J., Russell, G., Rind, D., Stone, P., Lacis, A., Lebedeff, S., Ruedy, R., & Travis, L. 1983. Efficient Three-Dimensional Global Models for Climate Studies: Models I and II. *Mon. Weath. Rev.*, **111**, 609–662.

Hansen, J., Sato, M., Nazarenko, L., Ruedy, R., Lacis, A., Koch, D., Tegen, I., Hall, T., Shindell, D., Santer, B., Stone, P., Novakov, T., Thomason, L., Wang, R., Wang, Y., Jacob, D., Hollandsworth, S., Bishop, L., Logan, J., Thompson, A., Stolarski, R., Lean, J., Willson, R., Levitus, S., Antonov, J., Rayner, N., Parker, D., & Christy, J. 2002. Climate Forcings in GISS SI2000 Simulations. *J. Geophys. Res.*, **107**, DOI 10.1029/2001JD001143.

Jones, P. D. 2000. *http://www.cru.uea.ac.uk/cru/data/temperat.htm*. University of East Anglia, Climate Research Unit.

Lean, J. 2000. Evolution of the Sun's Spectral Irradiance Since the Maunder Minimum. *Geophys. Res. Lett.*, **27**, 2421–2424.

Levitus, S., Antonov, J., Boyer, T. P., & Stephens, C. 2000. Warming of the World Ocean. *Science*, **287**, 2225–2229.

Mardia, K. V., Kent, K. T., & Bibby, J. M. 1979. *Multivariate Analysis*. Academic Press, New York.

Marshall, J.C., Hill, C., Perelman, L., & Adcroft, A. 1997. Hydrostatic, quasi-hydrostatic and non-hydrostatic ocean modeling. *J. Geophys. Res.*, **102**, 5,733 – 5,752.

Parker, D. E., Gordon, M., Cullum, D. P. N., Sexton, D. M. H., Folland, C. K., & Rayner, N. 1997. A new global gridded radiosonde temperature data base and recent temperature trends. *Geophys. Res. Lett.*, **24**, 1499–1502.

Ramankutty, N., & Foley, J. A. 1999. Estimating historical changes in global land cover: croplands from 1700 to 1992. *Global Biogeochemical Cycles*, **13**(4), 997–1027.

Sato, M., Hansen, J. E., McCormick, M. P., & Pollack, J. B. 1993. Stratospheric aerosol optical depths. *J. Geophys. Res.*, **98**, 22987–22994.

Smith, S. J., Andres, R., Conception, E., & Lurz, J. 2003. *Historical Sulfur Dioxide Emissions 1850-2000*. Tech. rept. ftp://jgcri.umd.edu/ssmith/Hist_SO2_Emissions/. Pacific Northwest National Laboratory, Joint Global Change Research Institute, 8400 Baltimore Avenue, College Park, Maryland 20740.

Sokolov, A. P., & Stone, P. H. 1998. A flexible climate model for use in integrated assessments. *Clim. Dyn.*, **14**, 291–303.

Sokolov, A.P., Schlosser, C.A., Dutkiewicz, S., Paltsev, S., Kicklighter, D.W., Jacoby, H.D., Prinn, R.G., Forest, C.E., Reilly, J., Wang, C., Felzer, B., Sarofim, M.C., Scott, J., Stone, P.H., Melillo, J.M., & Cohen, J. 2005. *The MIT Integrated Global System Model (IGSM) Version 2: Model Description and Baseline Evaluation, MIT JP Report 124*. Tech. rept. http://web.mit.edu/globalchange/www/MITJPSPGC_Rpt124.pdf. MIT, Joint Program on the Science and Policy of Global Change, Room E40-427, 77 Massachusetts Ave., Cambridge, MA 02139.

Stone, P. H., & Yao, M.-S. 1987. Development of a two-dimensional zonally averaged statistical-dynamical model. Part II: the role of eddy momentum fluxes in the general circulation and their parametrization. *J. Atmos. Sci.*, **44**(24), 3769–3786.

Stone, P. H., & Yao, M.-S. 1990. Development of a two-dimensional zonally averaged statistical-dynamical model. Part III: the parametrization of the eddy fluxes of heat and moisture. *J. Clim.*, **3**(7), 726–740.

Sun, S., & Hansen, J. E. 2003. Climate Simulations for 1951-2050 with a Coupled Atmosphere-Ocean Model. *J. Climate*, **16**, 2807–2826.

Wang, Y., & Jacob, D. 1998. Anthropogenic Forcing on Tropospheric Ozone and OH since Preindustrial Times. *J. Geophys. Res.*, **103**, 31123–31135.
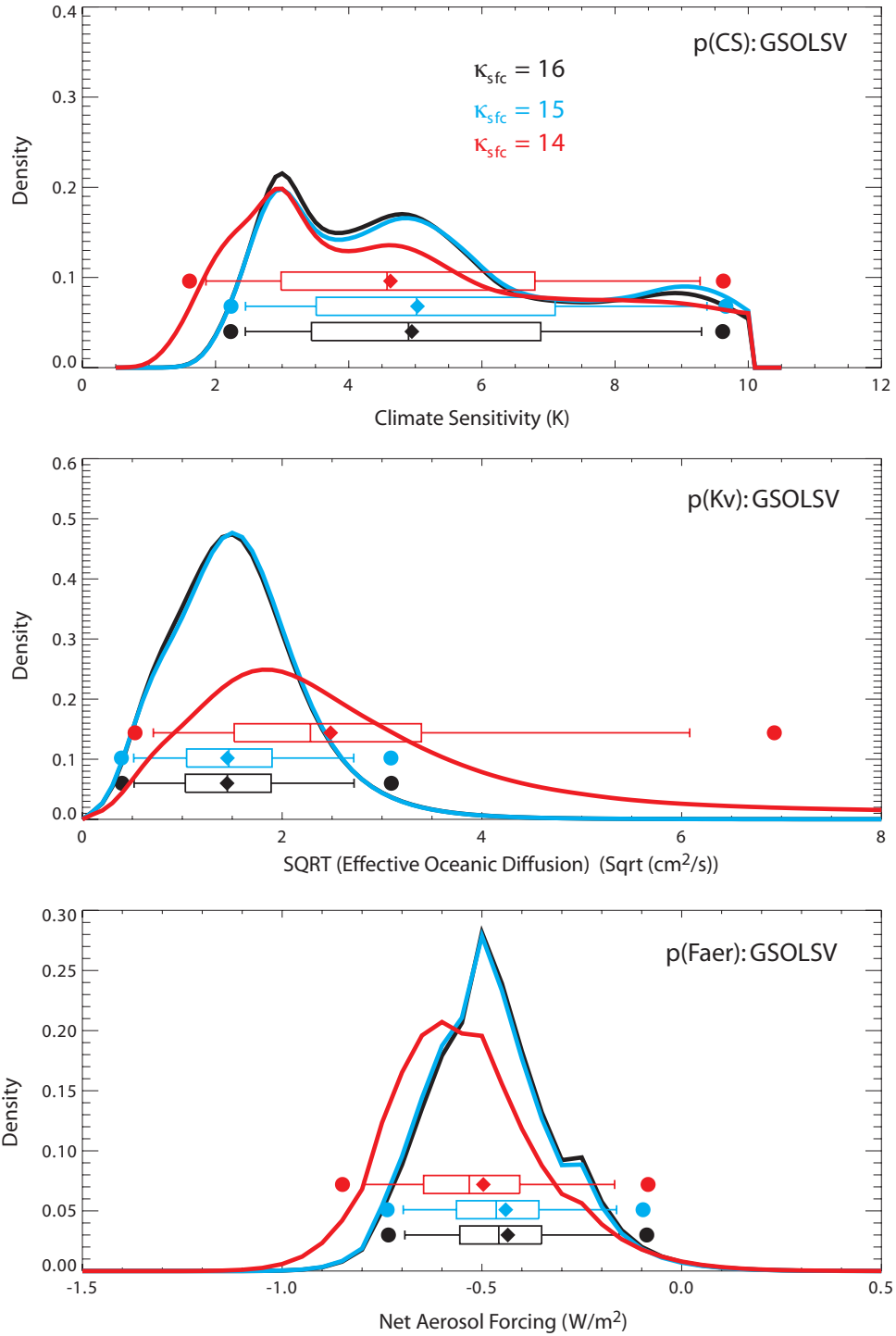
Figure S1: The marginal *posterior* probability density function for the three climate system properties for uniform priors while varying κ_{sfc} = 16, 18, 20 (a) and 14, 15, 16 (b) cases. This marginal distribution is estimated by integrating the density function over the remaining two parameters and renormalizing. The whisker plots indicate percentile boundaries for the 2.5 to 97.5 (dots), 5 to 95 (vertical bar ends), 25 to 75 (box ends), and 50 (vertical bar in box). The mean is indicated with the diamond and the mode is the peak in the distribution. The whisker plots correspond to the density function curves depicted the corresponding color.
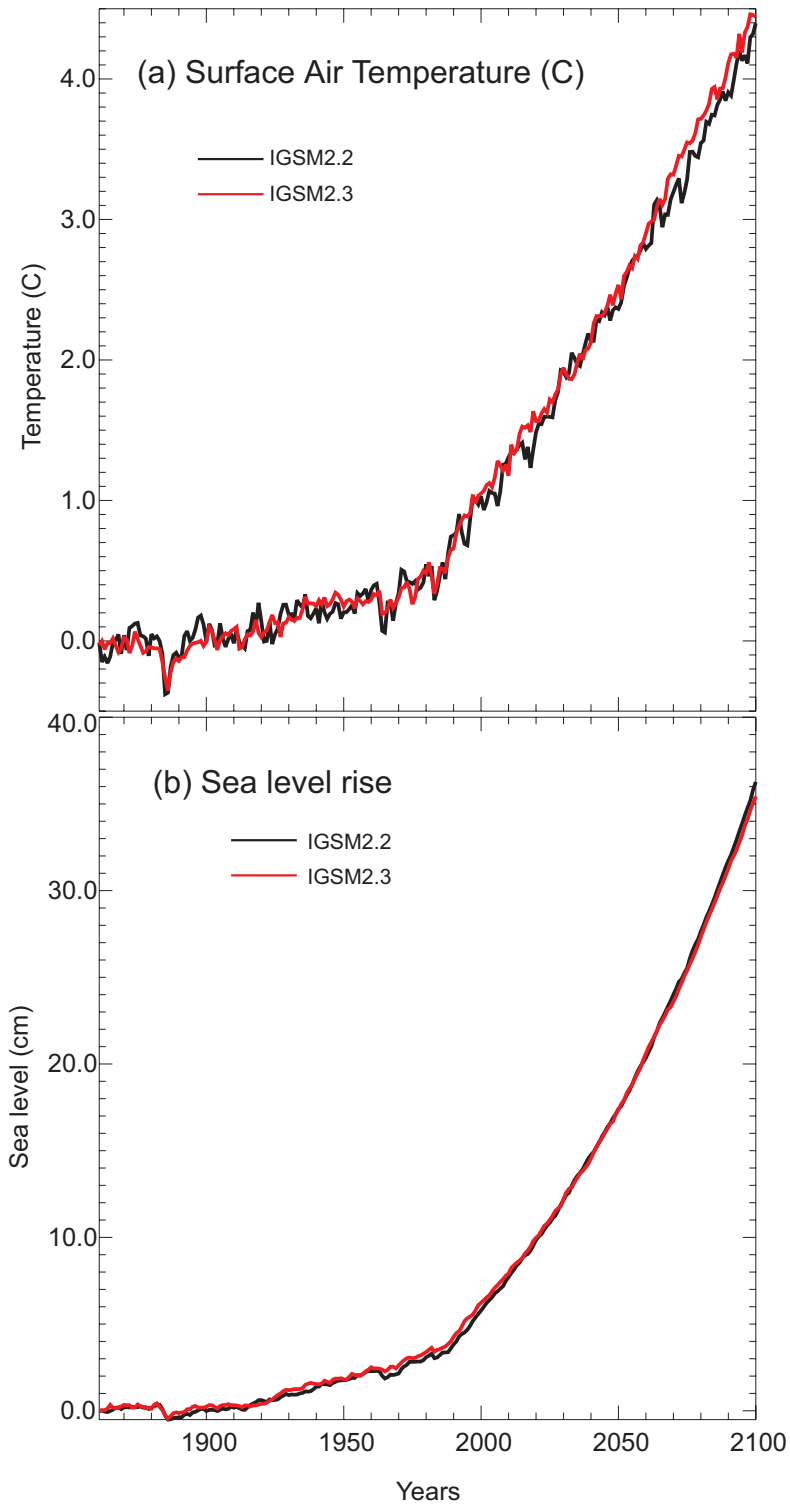
Figure S2: Changes in global-mean **(a)** annual-mean surface temperatures, and **(b)** sea-level rise due to thermal expansion from MIT 2D climate model with 2.5D Q-flux mixed layer model (IGSM2.2) as used in this study and with 3D ocean model (IGSM2.3) in response to 20th century GSOLSV forcings (1860-1990) and to MIT EPPA4 reference emissions scenario after 1990. (Sokolov *et al.* (2005) provides further details.)
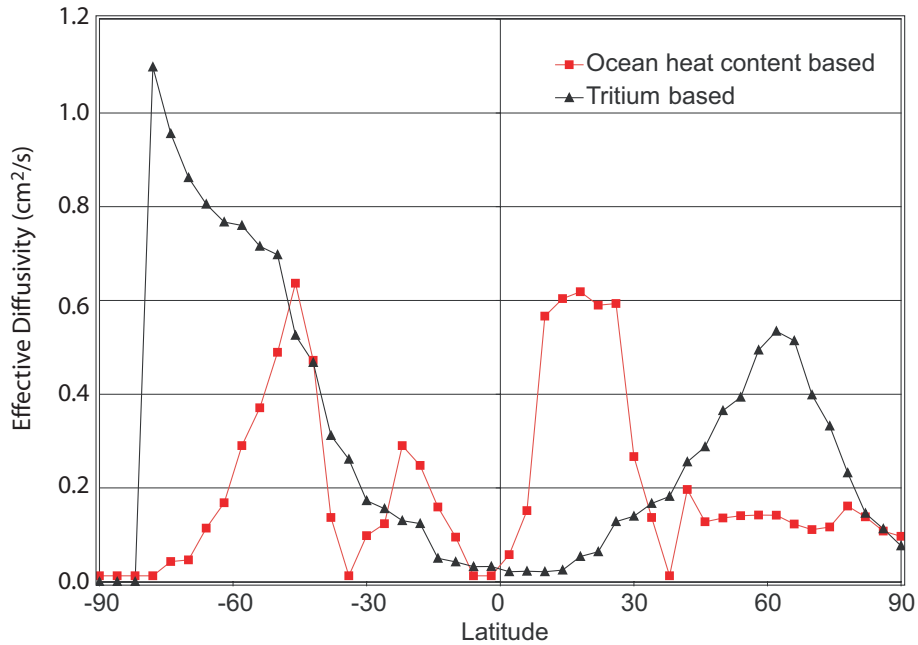
Figure S3: Latitude dependence of $K_v(\phi)$ for standard distribution based on mixing of tritium and new distribution based on observed changes in ocean heat content (Levitus *et al.*, 2000).
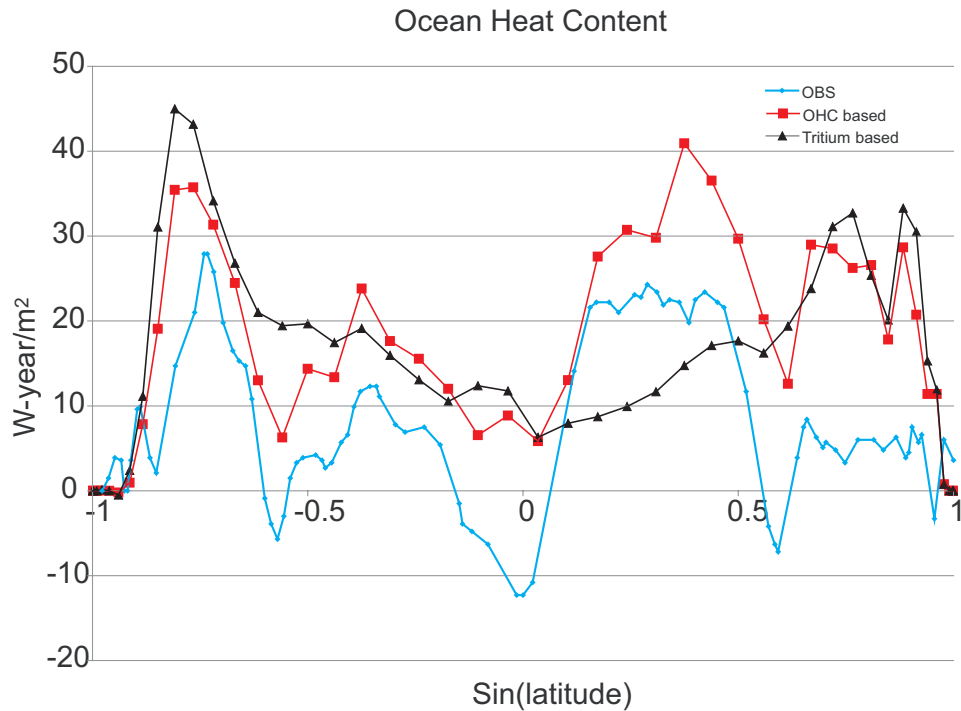
Figure S4: Changes in ocean heat content for observed (after Sun & Hansen, 2003) and GSOLSV simulations with old (tritium based) and new (ocean heat content based) $K_v(\phi)$ distributions. The total heat uptake in the simulations is larger than observed because the combination of S, K_v, and F_{aer} result in too much deep ocean heat uptake. Global-mean K_v are identical in both cases.
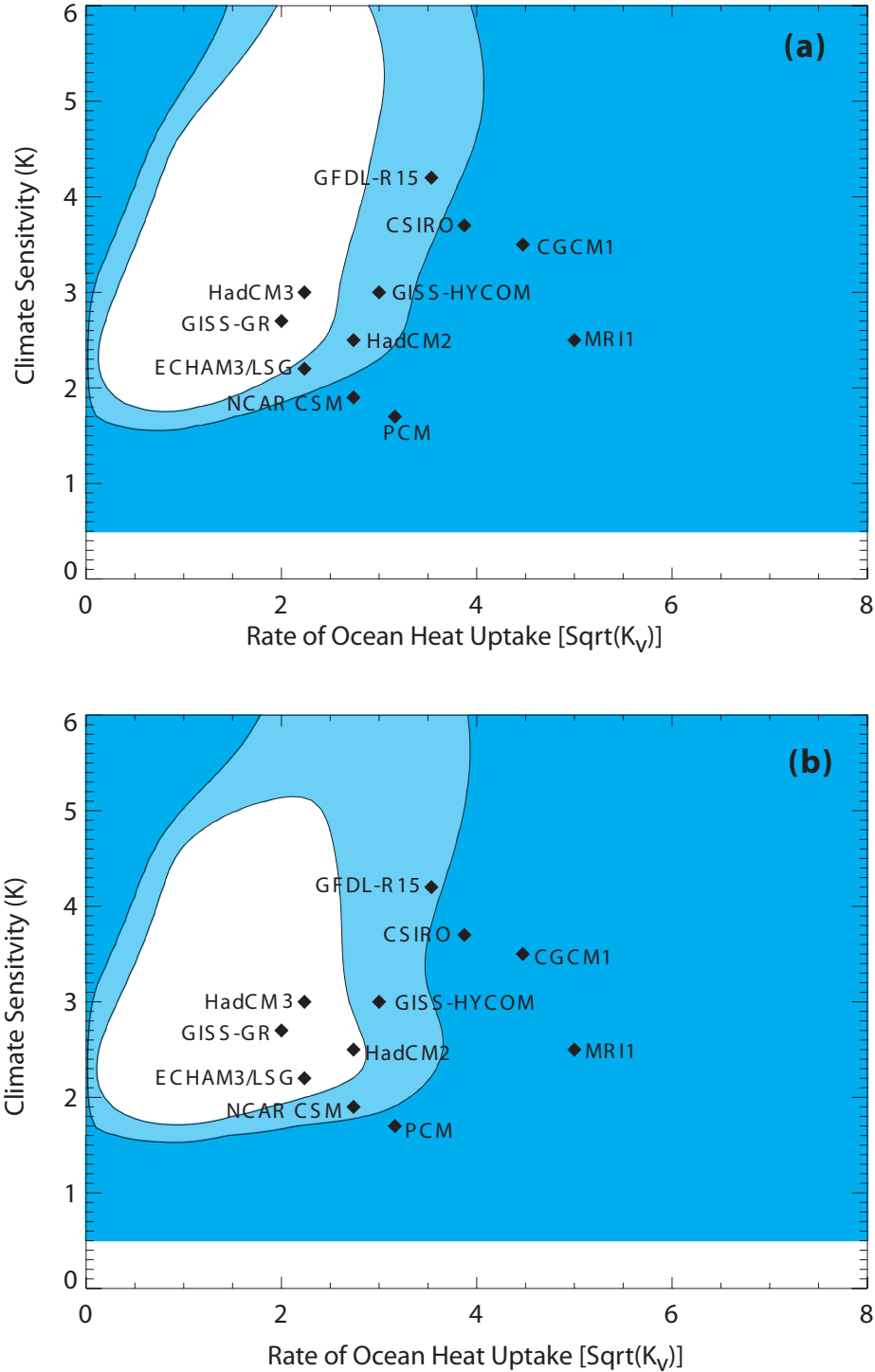
Figure S5: Conditional probability distributions, $p(\theta|T_{obs}, C_N, F_{aer} = -0.5 \text{ W/m}^2)$, based on GSOLSV simulations with **(a)** tritium based and **(b)** ocean heat content based $K_v(\phi)$ distributions. Blue shading indicates rejection regions of 10% (light) and 1% (dark) significance levels. The modes of the distributions are $S = 2.8$ and 2.6 K and $K_v = 2.0$ and 1.7 cm^2/s for (a) and (b), respectively. Uniform priors for all parameters were used in both distributions.
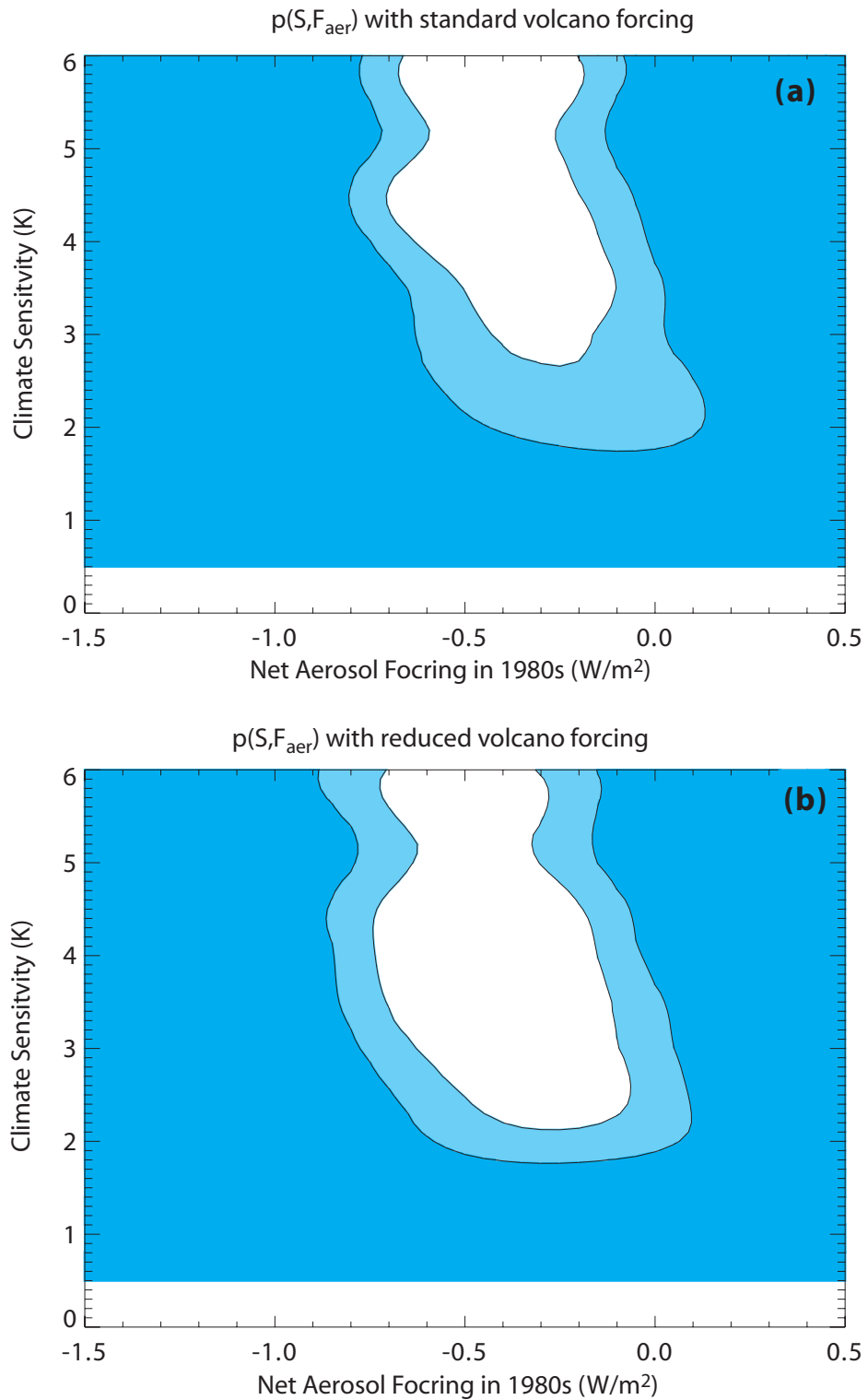
Figure S6: Conditional probability distributions, $p(\theta|T_{obs}, C_N, K_v = 4 \text{ cm}^2/\text{s})$, based on GSOLSV simulations with **(a)** standard volcanic forcing and **(b)** with volcanic forcing reduced by 25%. Blue shading indicates rejection regions of 10% (light) and 1% (dark) significance levels. Uniform priors for all parameters were used in both distributions.

REPORT SERIES of the MIT *Joint Program on the Science and Policy of Global Change*

Contact the Joint Program Office to request a copy. The Report Series is distributed at no charge.

REPORT SERIES of the MIT *Joint Program on the Science and Policy of Global Change*

Contact the Joint Program Office to request a copy. The Report Series is distributed at no charge.

REPORT SERIES of the MIT *Joint Program on the Science and Policy of Global Change*

Contact the Joint Program Office to request a copy. The Report Series is distributed at no charge.